

Effect of a Bulge on the Subharmonic Instability of Subsonic Boundary Layers

J. A. Masad* and A. H. Nayfeh†

Virginia Polytechnic Institute and State University, Blacksburg, Virginia 24061

The effect of a two-dimensional hump on the three-dimensional subharmonic instability of subsonic flow over a flat plate was investigated. The mean flow was calculated by using interacting boundary layers, thereby accounting for viscous/inviscid interactions and capturing separation bubbles. The results show that increasing the hump height produces an increase in the amplification factors of both the primary and subharmonic waves. When the hump causes separation, the growth rates of both the primary and subharmonic waves are considerably larger than those in the case of no separation. The effect of compressibility on reducing the amplification factors of the primary and subharmonic waves decreases as the hump height increases.

I. Introduction

THE performance of natural laminar flow (NFL) airfoils is critically dependent on the location of transition, which may be strongly influenced by surface imperfections. Although modern manufacturing techniques can provide smooth surfaces, some surface imperfections are unavoidable. These imperfections include, among others, waviness, bulges, dips, and steps. The mechanisms by which these imperfections cause transition include amplification of primary disturbances, shear-layer instability for separated flows, enhancement of secondary instabilities, amplification of crossflow vorticity, Görtler instability, enhancement of receptivity of freestream turbulence and acoustic disturbances, and any interaction between two or more of these mechanisms.

There are several experimental studies on the influence of surface imperfections on laminar-turbulent transition. However, most of these experiments were concerned with measuring the streamwise location of the onset of transition, rather than the growth and development of disturbances. This makes validation of proposed theoretical models a difficult task. One of the exceptions in this regard is the recent experimental study of Dovgal and Kozlov.¹ They investigated the influence of two-dimensional (2-D) humps, forward- and backward-facing steps on the stability of incompressible flow on a flat plate. They used a vibrating ribbon to introduce a disturbance with a specific frequency into the boundary layer and measured the streamwise growth and development of the disturbance as well as its distribution across the boundary layer. Their imperfections appear to be sharp rather than smooth. Forced (controlled) experiments studying the growth and development of disturbances in flows over smooth surface imperfections are needed.

To gain an insight into the physics of the instability of flows around surface imperfections, Nayfeh et al.² investigated the influence of 2-D humps and dips on the amplification of 2-D instability waves for incompressible flows. They correlated their results with the natural transition experiments of Walker and Greening (as reported by Fage³) and found that the calculated N factor corresponding to the experimental transition location is in the range of 7.4–10.0. They also found that the most dangerous frequency (the one which results in an N

factor equal to 9 in the shortest distance) is larger than that for the flow over a flat plate. Similar findings were later reported by Cebeci and Egan.⁴ Ragab et al.⁵ extended the work of Nayfeh et al.² to the case of subsonic flows over smooth 2-D backward-facing steps. In all of these theoretical studies, the interacting boundary-layer (IBL) formulation was used to calculate the mean flow over the imperfections, thereby accounting for viscous/inviscid interactions and capturing small separation bubbles. Ragab et al.⁵ validated the IBL approach by comparing its results for a backward-facing step with solutions of the compressible Navier-Stokes solver ARC2D. They compared the mean flows as well as their stability characteristics and found that, for the purpose of studying the stability of boundary layers over smooth surface imperfections, the IBL formulation is a viable alternative to the Navier-Stokes equations.

The secondary instability of subsonic flows is concerned with the parametric excitation of very low-amplitude three-dimensional (3-D) (secondary) disturbances by larger-amplitude 2-D (primary) disturbances. Depending on the relation between the frequencies and streamwise wave numbers of the exciting primary and excited secondary waves, one can distinguish between two types of resonances. When the frequency and streamwise wave number of the excited wave are equal to one-half those of the exciting wave, one has a subharmonic resonance. On the other hand, when the frequencies and streamwise wave numbers of the primary and secondary waves are equal, one has a fundamental parametric resonance. The subharmonic instability of incompressible boundary layers was modeled and studied by Herbert⁶ using the Floquet model. A comprehensive review of the secondary instability of incompressible boundary layers is given by Herbert.⁷

Nayfeh and Harper (as reported by Nayfeh⁸) extended the Floquet model and analyzed the spatial and temporal subharmonic instabilities of compressible flow over an adiabatic wall. They solved the spatial problem by using a shooting technique and presented results for subsonic, transonic, and supersonic flows. Nayfeh and Harper, however, neglected the interaction terms arising from the equation of state. El-Hady⁹ solved the spatial problem for subsonic and transonic boundary-layer flows. Masad and Nayfeh¹⁰ analyzed the subharmonic instability of compressible boundary layers. They presented results for subsonic, transonic, and supersonic flows. For supersonic flows, first- and second-mode primary waves were considered. Masad and Nayfeh¹⁰ found the subharmonic mode to be unstable over a wide band of frequencies. At the same amplitude of the primary wave, the subharmonic instability corresponding to second-mode primary waves was found to dominate that corresponding to first-mode primary waves.

Received Oct. 16, 1990; revision received Aug. 26, 1991; accepted for publication Oct. 8, 1991. Copyright © 1991 by A. H. Nayfeh. Published by the American Institute of Aeronautics and Astronautics, Inc., with permission.

*Research Scientist; currently at High Technology Corporation, Hampton, VA 23666.

†University Distinguished Professor, Department of Engineering Science and Mechanics.

Nayfeh et al.¹¹ investigated the effect of a 2-D hump on the 3-D subharmonic instability of incompressible flow over a flat plate. Their results show that increasing the hump height results in an increase in the amplification factors of both primary and subharmonic waves. When the hump causes separation, the growth rates of both primary and subharmonic waves were found to be considerably larger than those in the case of no separation.

In this paper, the influence of a 2-D hump on the 3-D subharmonic instability of subsonic flow over a flat plate is investigated. The freestream Mach numbers M_∞ of the considered flows are ≤ 0.8 so that there is at most one unstable primary wave for certain flow and stability parameters and that it is 2-D.¹² Therefore, the primary wave is taken in the form of a 2-D wave, whereas the secondary wave is taken in the form of a 3-D subharmonic wave. We point out here that in our earlier work,¹³ the calculations at $M_\infty = 0.0$ are for an adiabatic plate but all of the results at $M_\infty = 0.8$ are for a slightly cooled plate with $T_w/T_{ad} = 0.9$, where T_w and T_{ad} are the wall and adiabatic wall temperatures, respectively, which are made nondimensional with respect to the freestream temperature T_∞ . All of the results presented in this paper are for an adiabatic plate.

II. Problem Formulation and Methods of Solution

In Fig. 1, we show a small symmetric hump of height h^* and width $2b^*$ whose center is located at x_m^* . The distance L^* from the leading edge of the plate to the center of the hump is used as a reference quantity. Thus, in terms of nondimensional variables, the hump shape is given by

$$y = y^*/L^* = (h^*/L^*) f(\zeta) = hf(\zeta) \quad (1)$$

where

$$\zeta = (x^* - x_m^*)/b^* = (x - x_m)/b \quad (2)$$

We present numerical results for the Walker and Greening hump (see Ref. 3) described by

$$f(\zeta) = \begin{cases} 1 - 3\zeta^2 + 2|\zeta|^3 & \text{if } |\zeta| \leq 1 \\ 0 & \text{if } |\zeta| > 1 \end{cases} \quad (3)$$

The 2-D compressible laminar boundary layer over the plate and the hump is determined by solving the IBL equations. These equations account for upstream influence through the interaction of the viscous flow with the inviscid flow outside the boundary layer. Moreover, they are also capable of capturing separation bubbles without difficulties.⁵ Solutions are obtained by using a second-order finite difference method in which the grid spacings acknowledge the scalings predicted by triple-deck theory in the interaction region. For details of the IBL formulation for compressible flow as well as some aspects of the method of solution, we refer the reader to Ref. 5.

To formulate the subharmonic instability problem, we take the basic flow as the sum of the steady mean flow and a 2-D quasiparallel T-S wave, that is,

$$u_b = U_m(y) + A [\zeta_1(y)e^{i\theta} + cc] \quad (4)$$

$$v_b = A [\zeta_3(y)e^{i\theta} + cc] \quad (5)$$

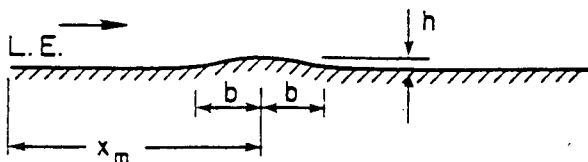


Fig. 1 Hump on a flat plate.

$$p_b = P_m + A [\zeta_4(y)e^{i\theta} + cc] \quad (6)$$

$$T_b = T_m(y) + A [\zeta_5(y)e^{i\theta} + cc] \quad (7)$$

$$\frac{\partial \theta}{\partial x} = \alpha_r, \quad \frac{\partial \theta}{\partial t} = -\omega \quad (8)$$

where cc stands for the complex conjugate of the preceding terms, α_r and ω are real, and $A = A_0 \exp(-\int \alpha_i dx)$ is approximated locally by a constant value. We normalize the eigenfunctions of the primary wave such that the maximum of the streamwise velocity disturbance ζ_1 is equal to $1/\sqrt{2}$ so that A denotes the rms amplitude of the primary wave.

We superimpose on this basic flow a 3-D unsteady quasiparallel disturbance, substitute the result into the Navier-Stokes equations, subtract the basic state, linearize, and obtain a system of partial-differential equations whose coefficients are independent of z and periodic in x and t . Consequently, the z variation can be separated and by using Floquet theory, we express the solution of these equations in the subharmonic case in either the form

$$(u, v, p, T, \rho) = e^{\sigma_x x + \sigma_t t} \cos \beta z [\{\xi_1, \xi_3, \xi_4, \xi_5, \xi_9\} e^{1/2 i \theta} + cc] + \{\xi_1, \xi_3, \xi_4, \xi_5, \xi_9\} e^{-1/2 i \theta} + cc] \quad (9)$$

$$w = e^{\sigma_x x + \sigma_t t} \sin \beta z [\xi_7 e^{1/2 i \theta} + \xi_7 e^{-1/2 i \theta} + cc] \quad (10)$$

or the form

$$(u, v, p, T, \rho) = e^{\sigma_x x + \sigma_t t} \sin \beta z [\{\xi_1, \xi_3, \xi_4, \xi_5, \xi_9\} e^{1/2 i \theta} + \{\xi_1, \xi_3, \xi_4, \xi_5, \xi_9\} e^{-1/2 i \theta} + cc] \quad (11)$$

$$w = e^{\sigma_x x + \sigma_t t} \cos \beta_z [\xi_7 e^{1/2 i \theta} + \xi_7 e^{-1/2 i \theta}] \quad (12)$$

For the case of temporal stability, $\sigma_x = 0$ and $\sigma_t \neq 0$, whereas for the case of spatial stability $\sigma_t = 0$ and $\sigma_x \neq 0$. The excited subharmonic wave is a linear combination of the forms given by Eqs. (9) and (10) and Eqs. (11) and (12). The form of the solution given by either of these forms consists of a pair of 3-D propagating waves that form a spanwise standing wave. They are 90 deg out of phase. For tuned modes ξ_m is equal to $\bar{\xi}_m$, the complex conjugate of ξ_m , and σ_x and σ_t are real. This the case that we are considering in this paper.

The details of analyzing the primary and subharmonic instabilities of compressible flows as well as an outline of a finite difference method of solution for the resulting problems are given by Masad and Nayfeh.¹⁰

III. Results

Throughout this paper, $Re = U_\infty^* L^* / \nu_\infty^*$ denotes the Reynolds number based on L^* , whereas $R = U_\infty^* \delta_r^* / \nu_\infty^*$ denotes the Reynolds number based on the length scale $\delta_r^* = \sqrt{\nu_\infty^* x^* / U_\infty^*}$, where x^* is the dimensional distance from the leading edge of the plate to the location where the stability calculations are performed, ν_∞^* is the dimensional freestream kinematic viscosity, and U_∞^* is the dimensional freestream velocity of the flow. Thus, $R = \sqrt{x} Re$, where $x = x^*/L^*$. The frequency $F = \omega^* \nu_\infty^* / U_\infty^*$, where ω^* is the dimensional circular frequency of the disturbance, remains constant as the wave propagates downstream; F_{2D} refers to the value of F for the 2-D primary wave. Because the mean flow is 2-D and stationary, the dimensional spanwise wave number β^* and hence $B = 1000 \beta^* \nu_\infty^* / U_\infty^*$ remain constant as the wave propagates downstream. For all of the results presented in this paper, $Re = 10^6$, the hump is centered at $x = 1.0$ and extends between $x = 0.9$ and 1.1 , and the hump height \bar{h} is related to h through $\bar{h} = h\sqrt{Re} = 1000h$. Moreover, the freestream temperature T_∞ is kept constant and equal to 300 K, the Prandtl number is kept constant and equal

to 0.72, and the variation of viscosity with temperature is given by the Sutherland formula.

We used spatial stability theory for primary waves so that ω is real and $\alpha = \alpha_r + i\alpha_i$ is complex, where α_r is the streamwise wave number and $-\alpha_i$ is the growth rate of the primary wave. For subharmonic waves, we used both spatial ($\sigma_x \neq 0$ but $\sigma_t = 0$) and temporal ($\sigma_t \neq 0$ but $\sigma_x = 0$) stability theories.

Before presenting results for the subharmonic instability, we justify the quasiparallel assumption. Although this assumption has been justified for conventional aerodynamic surfaces, one might question its validity for the configuration under consideration. Because the wavelengths of the disturbances for the geometrical and flow parameters of our configuration are the same order as those of the flow over a flat plate without imperfections, the nonparallel effects are second-order quantities and to first order the disturbance can be considered to be quasiparallel. Moreover, the direct numerical simulations of Bestek et al.¹⁴ and the experimental results of Dovgal and Kozlov¹ support the quasiparallel assumption. Bestek et al.¹⁴ investigated the influence of a 2-D smooth backward-facing step on the spatial development of a Tollmien-Schlichting wave by numerically integrating the Navier-Stokes equations using a finite difference scheme. The growth rates obtained by the direct numerical simulation are in excellent agreement with those obtained by a quasiparallel theory. Dovgal and Kozlov experimentally investigated the stability characteristics of flows over humps and backward- and forward-facing steps. The experimentally determined transverse and streamwise development of the disturbances ahead, inside, and after the separation bubble is similar to those obtained here and in Refs. 2 and 5 by a quasiparallel theory. Our theoretically predicted variation of the integral of the growth rate over a forward-facing step with streamwise location is in good agreement with their experimental results, as shown in Fig. 2.

To study the effect of compressibility on the stability characteristics, one needs first to determine its influence on the mean flow. In Fig. 3, we compare the streamwise distributions of the pressure C_p and friction C_f coefficients over a hump that induces a separation bubble for $M_\infty = 0.0$ and 0.8. There is an adverse pressure gradient ahead of the hump; it is followed by a favorable pressure gradient extending over a very short region and the pressure gradient becomes adverse again, causing the boundary layer to separate. Generally speaking, one expects the disturbance to be unstable ahead of the hump, become stable over the short favorable pressure-gradient region, and then turn unstable in the separation region. This general behavior has been predicted for different humps at different Reynolds numbers and over a wide range of frequencies by Nahfeh et al.² Comparing the skin-friction distributions for $M_\infty = 0.0$ and 0.8, we conclude that increasing the Mach number increases the streamwise extent of the separation bubble.

Next, we consider the effect of compressibility on the size of the separation bubble as the height of the hump changes. In Fig. 4a, we show variation of the streamwise locations of separation and reattachment with hump height for $M_\infty = 0.0$ and 0.8. For a given Mach number M_∞ and a given hump height $\bar{h} = h\sqrt{Re} = 1000h$, the left branch corresponds to the separation location, whereas the right branch corresponds to the reattachment location. As the Mach number increases, the hump height that induces separation decreases. Moreover, as the Mach number increases, the separation location moves slightly upstream, whereas the reattachment location moves significantly downstream. In Fig. 4b, we show variation of the maximum normal extent of the separation bubble with hump height for $M_\infty = 0.0$ and 0.8. It is clear that increasing the Mach number results in an increase in the size and streamwise extent of the separation bubble, which enhances the shear-layer instability. However, for given mean-flow profiles, compressibility is stabilizing. Therefore, the overall effect of compressibility depends on the relative strength of these competing mechanisms.

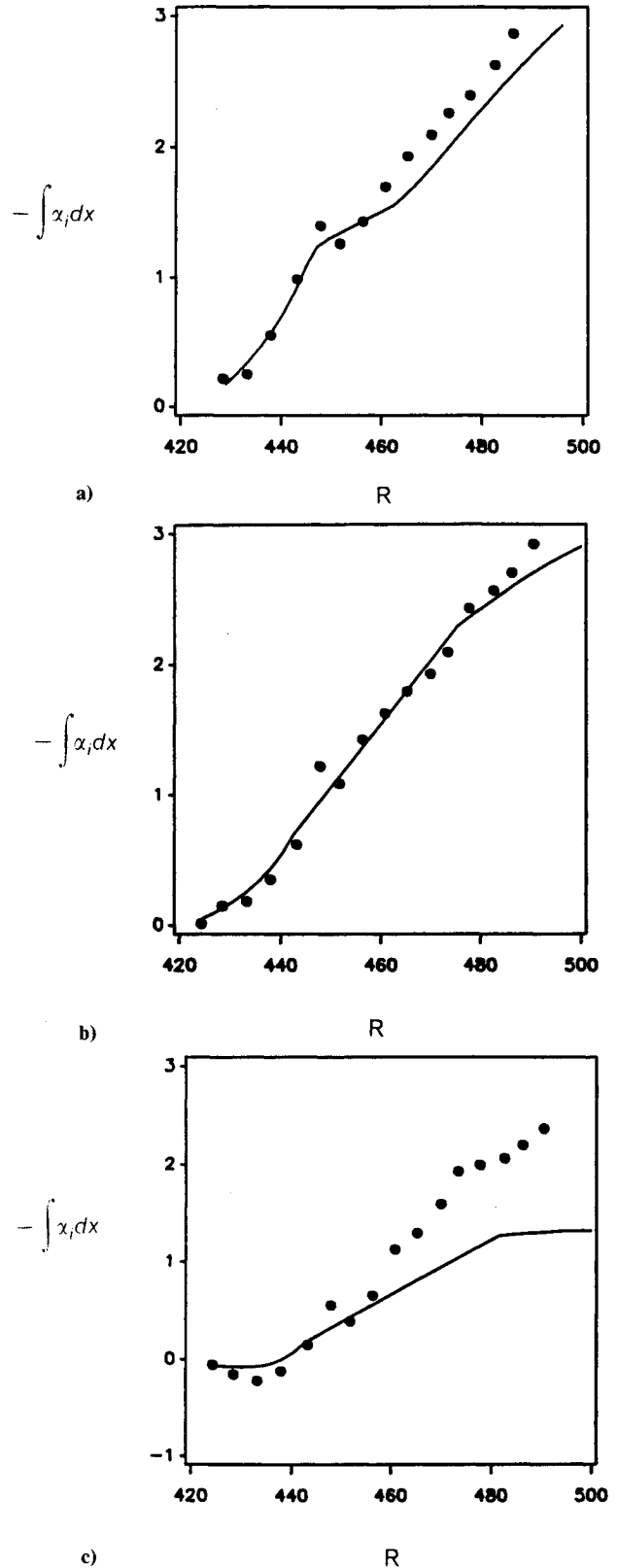
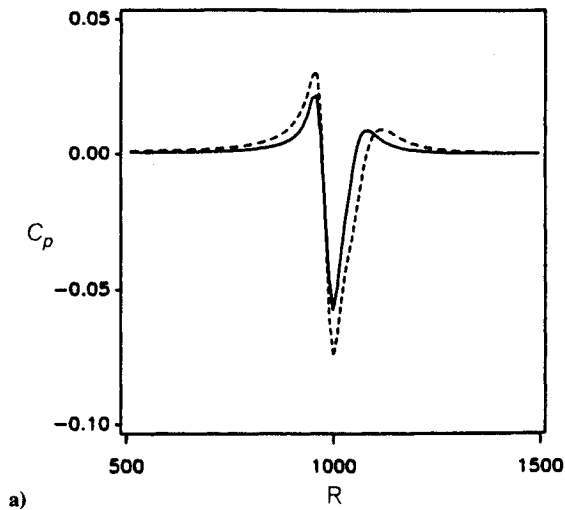
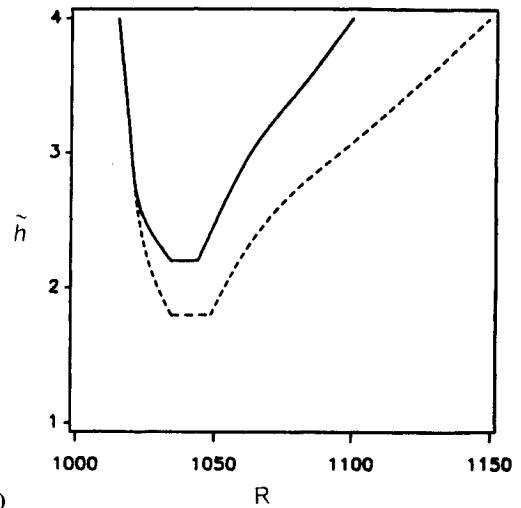


Fig. 2 Variation of $-\int \alpha_i dx$ with R for a flow over a forward-facing step at $Re = 2 \times 10^5$, step height = 0.0044, and step slope = 10. (—) theoretical results and (⊕) experimental data of Dovgal and Kozlov¹: a) $F = 157 \times 10^{-6}$; b) $F = 199 \times 10^{-6}$, and c) $F = 246 \times 10^{-6}$.

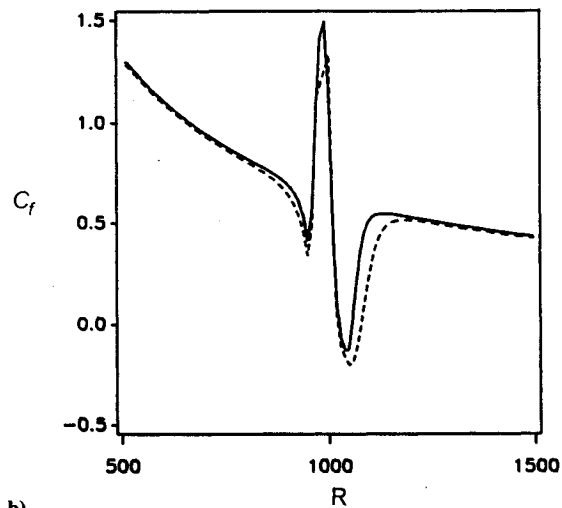
To determine the effects of compressibility and hump height on the primary and subharmonic modes, we performed a local stability analysis of the mean-flow profiles at $x = 1.1$ (i.e., $R = 1048.81$) for humps with $\bar{h} = 1.0, 1.6,$ and 2.5 for a fixed value of $B = 0.2$. The hump corresponding to $\bar{h} = 1.0$, does not induce any flow separation, whereas that corresponding to



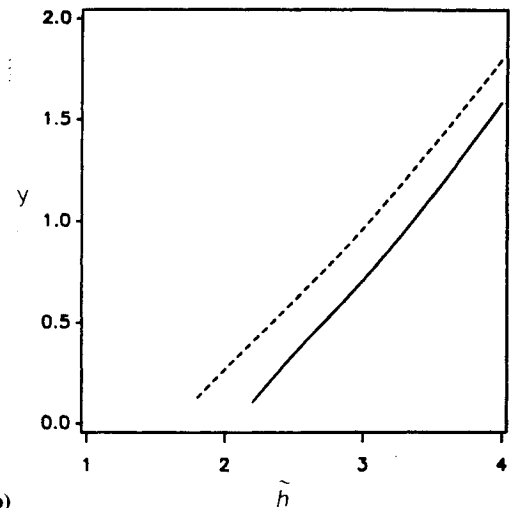
a)



a)



b)



b)

Fig. 3 Streamwise distributions of pressure C_p and skin-friction C_f coefficients for a flow over a hump at $Re = 10^6$ and $\tilde{h} = 2.5$: (—) $M_\infty = 0.0$ and (---) $M_\infty = 0.8$.

Fig. 4 Variation of the a) streamwise locations of separation and reattachment and b) maximum normal extent of the separation bubble with hump height when $Re = 10^6$: (—) $M_\infty = 0.0$ and (---) $M_\infty = 0.8$.

$\tilde{h} = 1.6$ shows incipient separation at $M_\infty = 0.8$. The hump corresponding to $\tilde{h} = 2.5$ induces a separation bubble. For $A_{rms} = 0.01U_\infty^*$, variations of the growth rates of the primary and subharmonic waves with F_{2D} at $M_\infty = 0.0$ and 0.8 are shown in Figs. 5a and 5b, respectively. Both the primary and subharmonic waves are amplified over a wide band of frequencies and there is a sharp cutoff at low frequencies. Moreover, compressibility is destabilizing at low frequencies but stabilizing at high frequencies. As the hump height increases, the frequency of the most amplified primary wave is shifted to a higher frequency.

We also performed a local stability analysis of the mean-flow profiles at $x = 1.1$ for humps with $\tilde{h} = 0.0, 1.0, 1.6,$ and 2.5 for a fixed value of $F_{2D} = 83 \times 10^{-6}$. Variation of the growth rate of the subharmonic wave with B is shown in Fig. 6. There is a broad band of unstable spanwise wave numbers and a sharp cutoff at low spanwise wave numbers, which are characteristics of the subharmonic wave. Compressibility is stabilizing for all heights and spanwise wave numbers. Increasing the hump height results in an increase in the growth rate of the subharmonic wave and a shift in the most amplified spanwise wave number towards a lower value for both incompressible and compressible flows.

We then considered the streamwise variation of the growth rates of the primary and subharmonic waves for the hump heights $\tilde{h} = 1.0, 1.6,$ and 2.5 . We started the stability calculations at $x = 1.03$, a small distance downstream of the center of the humps, and terminated the calculations at a value of $R = \sqrt{x}Re = 1000 \sqrt{x} \leq 1200$. At the initial station, we assumed that $A = A_0$ and choose a value of B . Then we marched downstream and computed the growth rates of both the primary and subharmonic waves. Variation of the growth rates of the primary and subharmonic waves for the three humps at $F_{2D} = 90 \times 10^{-6}$ is shown in Figs. 7a and 7b. Near the hump compressibility has a stabilizing influence, which becomes destabilizing as the disturbance propagates some distance downstream. For the small hump $\tilde{h} = 1.0$, the growth rates are small. However, as the hump height increases, the growth rates increase for both compressible and incompressible flows. The case with separation bubble ($\tilde{h} = 2.5$) shows considerable amplification over a short distance. Because, as shown in Fig. 7c, the rms amplitudes of the primary waves reach large values downstream, the subharmonic instability may not dominate the fundamental instability there.⁷ Moreover, at these large amplitudes the distortion of the mean flow might not be negligible and hence should be accounted for in the model. In

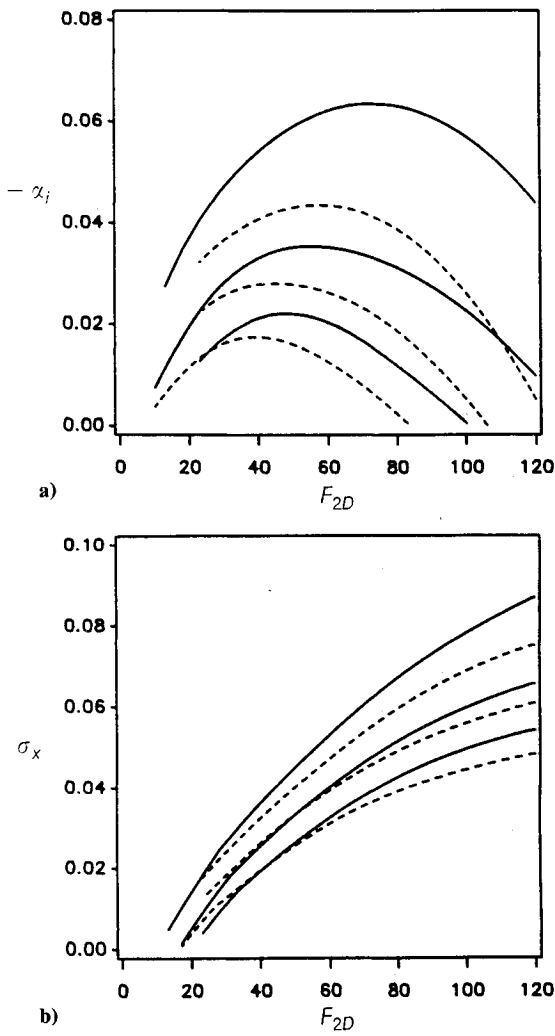


Fig. 5 Variations of the a) primary growth rate $-\alpha_i$ and b) subharmonic growth rate σ_x with the frequency F_{2D} of the primary wave at $R = 1048.81$, $B = 0.2$, $x = 1.1$, and $A_{rms} = 0.01$: (—) $M_\infty = 0.0$ and (---) $M_\infty = 0.8$. The hump height \bar{h} proceeding downward is 2.5, 1.6, and 1.0.

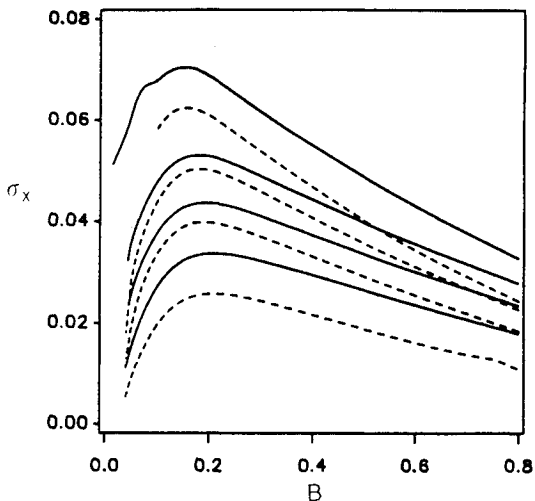


Fig. 6 Variation of the subharmonic growth rate σ_x with spanwise wave number at $R = 1048.81$, $F_{2D} = 83 \times 10^{-6}$, $x = 1.1$, and $A_{rms} = 0.01$: (—) $M_\infty = 0.0$ and (---) $M_\infty = 0.8$. The hump height \bar{h} proceeding downward is 2.5, 1.6, 1.0, and 0.0.

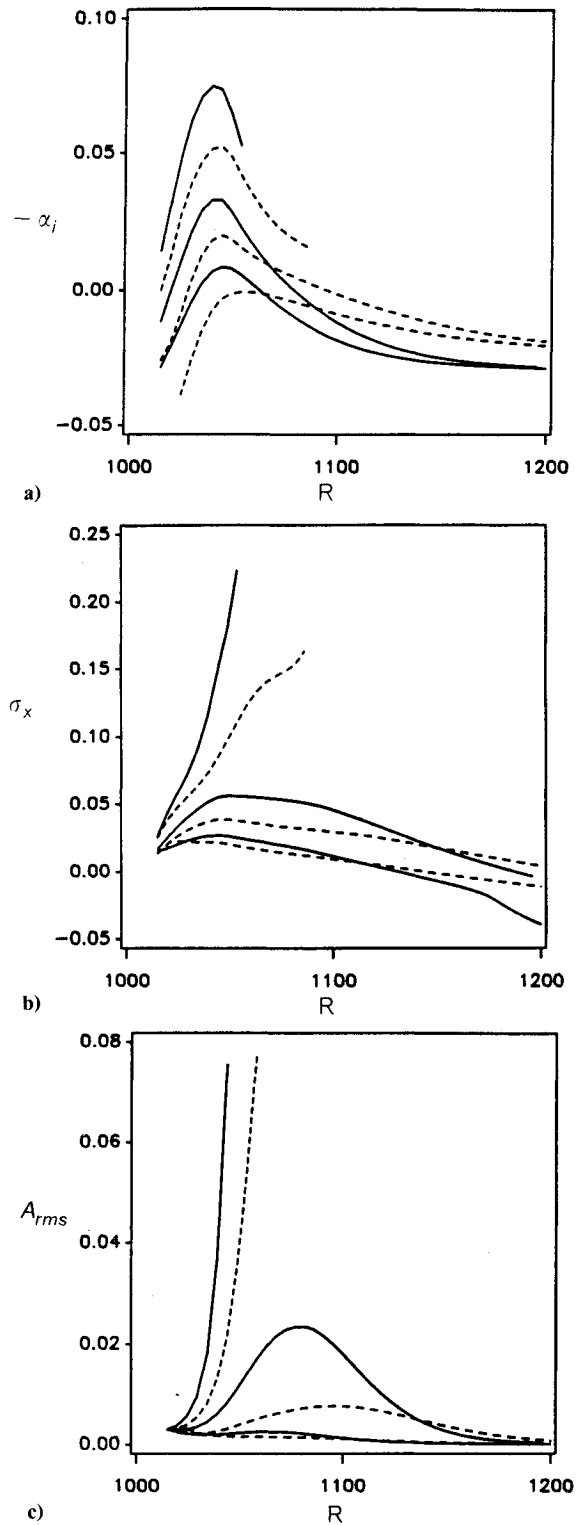


Fig. 7 Streamwise variations of the a) growth rate $-\alpha_i$ of the primary wave, b) growth rate σ_x of the subharmonic wave, and c) rms amplitude of the primary wave for $B = 0.2$, $F_{2D} = 90 \times 10^{-6}$, and $A_{rms} = 0.003$ at the initial station $x = 1.03$; (—) $M_\infty = 0.0$ and (---) $M_\infty = 0.8$. The hump height \bar{h} proceeding downward is 2.5, 1.6, and 1.0.

addition, at these large amplitudes the growth rates and hence the amplitude of the subharmonic wave (Fig. 7b) may be very large, which may invalidate the Floquet analysis because the subharmonic wave is expected to pump part of its energy back into the primary wave causing it to become more unstable.^{15,16} The trends at $F_{2D} = 90 \times 10^{-6}$ which are shown in Fig. 7 persist at $F_{2D} = 45 \times 10^{-6}$. The latter results are not shown in this paper.

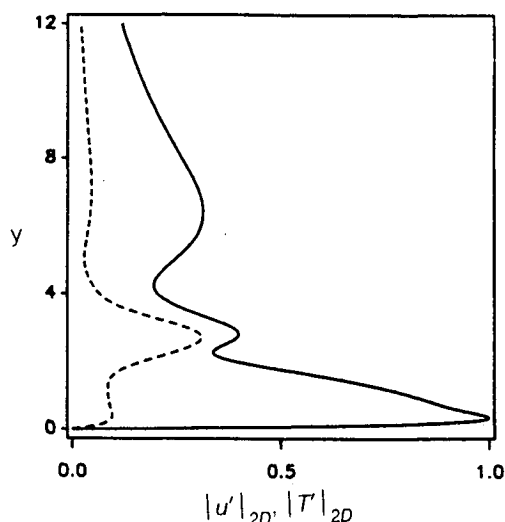


Fig. 8 Variation of the magnitudes of the (—) streamwise velocity and (---) temperature primary disturbances across the boundary layer for a flow over a hump with $\bar{h} = 2.5$ when $M_\infty = 0.8$, $R = 1048.81$, and $F_{2D} = 83 \times 10^{-6}$.

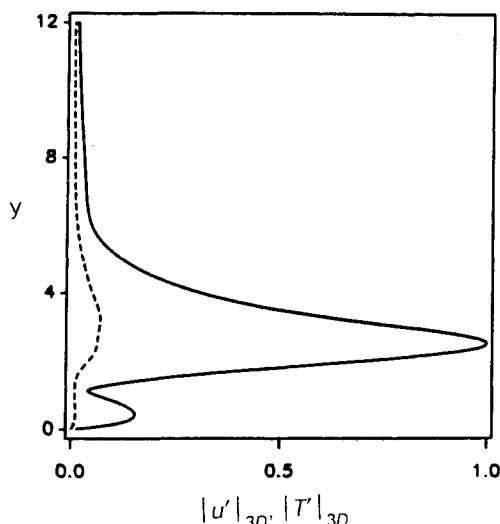


Fig. 9 Variation of the magnitudes of the (—) streamwise velocity and (---) temperature of the subharmonic disturbance across the boundary layer for a flow over a hump with $\bar{h} = 2.5$ when $M_\infty = 0.8$, $R = 1048.81$, $F_{2D} = 83 \times 10^{-6}$, $B = 0.2$, and $A_{rms} = 0.01$.

Variation of the magnitudes of the streamwise velocity and temperature primary disturbances across the boundary layer for a separating flow over a hump is shown in Fig. 8. The freestream Mach number of the flow is $M_\infty = 0.8$ and $F_{2D} = 83 \times 10^{-6}$. The streamwise velocity has a three-peak character, as predicted theoretically for incompressible separating flows by Nayfeh et al.² and found experimentally by Dovgal and Kozlov,¹ and numerically by Bestek et al.¹⁴ The temperature disturbance distribution has also three peaks. The middle peaks are related to the shear-layer instability mechanism.

We then investigated the effect of separation on the distribution of the magnitudes of the streamwise velocity and temperature of the subharmonic disturbance across the boundary layer. The results, which are shown in Fig. 9, indicate that the streamwise velocity of the subharmonic disturbance has two peaks corresponding to the viscous and shear-layer peaks of the primary disturbance.

Finally, we relate the temporal and spatial instabilities. Herbert and Bertolotti (Ref. 17) showed that temporal subhar-

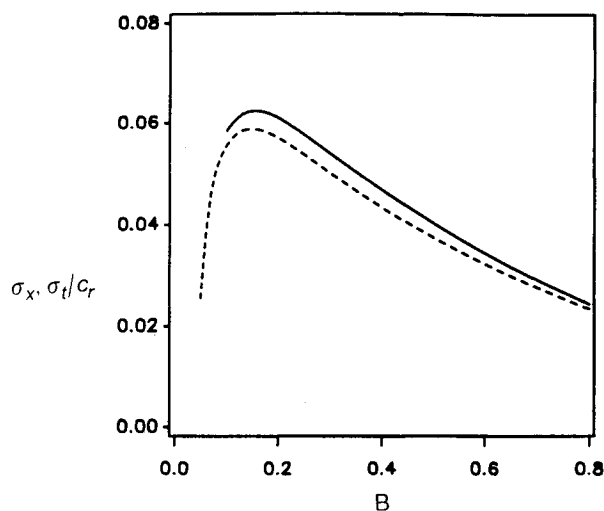


Fig. 10 Variation of the (—) calculated spatial growth rate σ_x and (---) transformed growth rate σ_t/c_r of the subharmonic wave with spanwise wave number B for a flow over a hump with $\bar{h} = 2.5$ when $R = 1048.81$, $F_{2D} = 83 \times 10^{-6}$, $M_\infty = 0.8$, and $A_{rms} = 0.01$.

monic growth rates σ_t of incompressible flow over a flat plate can be converted with a good accuracy to spatial growth rates σ_x by dividing them by the real part of the phase speed c_r . In Fig. 10, we compare the spatial growth rates σ_x of a separating flow at $M_\infty = 0.8$ calculated from the eigenvalue problem with the growth rates σ_t/c_r calculated from the temporal growth rates. The accuracy of the transformations is good and gets better as the growth rate decreases.

IV. Conclusions

The effect of a 2-D hump on the 3-D subharmonic instability of subsonic flow over a flat plate was investigated. The mean flow was calculated by using interacting boundary layers, thereby accounting for the viscous/inviscid interaction. The effect of the hump height, compressibility, spanwise wave number, and frequency on the growth rates of the primary and subharmonic waves was determined. The effect of the hump height and compressibility on the growth rates and amplification factors of the primary and subharmonic waves was also determined. It is found that variation of the subharmonic growth rate with spanwise wave number has the common features of a broad band of unstable spanwise wave numbers and a sharp cutoff at low spanwise wave numbers. The results show that increasing the hump height results in a shift of the most amplified spanwise wave number towards a lower value. The results also show that, in the case of subharmonic waves, there is a broadband of unstable frequencies and the most amplified frequency shifts towards a higher value as the height of the hump increases.

The results show that, although compressibility significantly reduces the amplification factor in the case of a smooth surface, this stabilizing effect decreases as the hump height increases because compressibility increases the transverse as well as the streamwise extents of the separation bubble. In the absence of separation, it is found that increasing the hump height results in an increase in the amplification factors for both the primary and subharmonic waves. In the case of separation, the amplification factors are considerably increased.

Acknowledgment

This work was supported by the Office of Naval Research under Grant N00014-85-K-0011/NR 4325201.

References

1. Dovgal, A. V., and Kozlov, V. V., "Hydrodynamic Instability and Receptivity of Small Scale Separation Regions," *Laminar-Turbulent*

Transition, edited by D. Arnal and R. Michel, Springer, Berlin, 1990, pp. 523-531.

²Nayfeh, A. H., Ragab, S. A., and Al-Maaitah, A. A., "Effect of Bulges on the Stability of Boundary-Layers," *Physics of Fluids*, Vol. 31, 1988, pp. 796-806.

³Fage, A., "The Smallest Size of Spanwise Surface Corrugation Which Affect Boundary-Layer Transition on an Airfoil," British Aeronautical Research Council, Rept. and Memoranda 2120, 1943.

⁴Cebeci, T., and Egan, D. A., "Effect of Wave-Like Roughness on Transition," *AIAA Journal*, Vol. 27, 1989, pp. 870-875.

⁵Ragab, S. A., Nayfeh, A. H., and Krishna, R. C., "Stability of Compressible Boundary Layers over Smooth Backward- and Forward-Facing Steps," AIAA Paper 90-1450, 1990.

⁶Herbert, Th., "Analysis of the Subharmonic Route to Transition in Boundary Layers," AIAA Paper 84-0009, 1984.

⁷Herbert, Th., "Secondary Instability of Boundary Layers," *Annual Review of Fluid Mechanics*, Vol. 20, 1988, pp. 487-526.

⁸Nayfeh, A. H., "Stability of Compressible Boundary Layers," *Transonic Symposium: Theory, Application, and Experiment*, NASA CP 3020, Vol. 1, NASA Langley Research Center, Hampton, VA, 1988, pp. 629-689.

⁹El-Hady, N. M., "Secondary Instability of Compressible Boundary Layer to Subharmonic Three-Dimensional Disturbances," AIAA Paper 89-0035, 1989.

¹⁰Masad, J. A., and Nayfeh, A. H., "Subharmonic Instability of Compressible Boundary Layers," *Physics of Fluids*, Vol. A2, No. 8, 1990, pp. 1380-1392.

¹¹Nayfeh, A. H., Ragab, S. A., and Masad, J. A., "Effect of a Bulge on the Subharmonic Instability in Boundary Layers," *Physics of Fluids*, Vol. A2, No. 6, 1990, pp. 937-948.

¹²Mack, L. M., "Boundary-Layer Stability Theory," Jet Propulsion Lab., Document 900-277, Rev. A, California Inst. of Technology, Pasadena, CA.

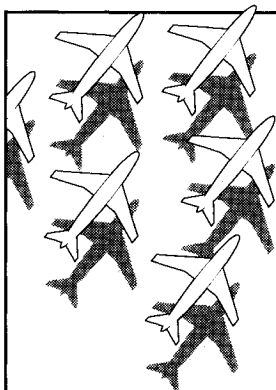
¹³Masad, J. A., and Nayfeh, A. H., "Effect of a Bulge on the Subharmonic Instability of Compressible Boundary Layers," AIAA Paper 90-1526, 1990.

¹⁴Bestek, H., Gruber, K., and Fasel, H., "Numerical Investigation of Unsteady Laminar Boundary Layer Flows over Backward-Facing Steps," Fourth Asian Congress of Fluid Mechanics, Hong Kong, Aug. 19-23, 1989.

¹⁵Herbert, Th., "Three-Dimensional Phenomena in the Transitional Flat-Plate Boundary Layer," AIAA Paper 85-0489, 1985.

¹⁶Crouch, J. D., "The Nonlinear Evolution of Secondary Instabilities in Boundary Layers," Ph.D. Thesis, Virginia Polytechnic Inst. and State Univ., Blacksburg, VA, 1988.

¹⁷Bertolotti, F. B., "Temporal and Spatial Growth of Subharmonic Disturbances in Falkner-Skan Flows," M.S. Thesis, Virginia Polytechnic Inst. and State Univ., Blacksburg, VA, 1985.



Recommended Reading from Progress in Astronautics and Aeronautics

Applied Computational Aerodynamics

P.A. Henne, editor

Leading industry engineers show applications of modern computational aerodynamics to aircraft design, emphasizing recent studies and developments. Applications treated range from classical airfoil studies to the aerodynamic evaluation of complete aircraft. Contains twenty-five chapters, in eight sections: History; Computational Aerodynamic Schemes; Airfoils, Wings, and Wing Bodies; High-Lift Systems; Propulsion Systems; Rotors; Complex Configurations; Forecast. Includes over 900 references and 650 graphs, illustrations, tables, and charts, plus 42 full-color plates.

1990, 925 pp, illus, Hardback, ISBN 0-930403-69-X
 AIAA Members \$69.95, Nonmembers \$103.95
 Order #: V-125 (830)

Place your order today! Call 1-800/682-AIAA



American Institute of Aeronautics and Astronautics
 Publications Customer Service, 9 Jay Gould Ct., P.O. Box 753, Waldorf, MD 20604
 Phone 301/645-5643, Dept. 415, FAX 301/843-0159

Sales Tax: CA residents, 8.25%; DC, 6%. For shipping and handling add \$4.75 for 1-4 books (call for rates for higher quantities). Orders under \$50.00 must be prepaid. Please allow 4 weeks for delivery. Prices are subject to change without notice. Returns will be accepted within 15 days.

